



**HAL**  
open science

# Hydrocarbon Fuels from Sequential Hydrothermal Liquefaction (HTL) of Lignite and Catalytic Upgrading of Crude Oil

Nuno Batalha, Ruben Checa, Chantal Lorentz, Pavel Afanasiev, Krzysztof Stańczyk, Krzysztof Kapusta, Dorothée Laurenti, Christophe Geantet

► **To cite this version:**

Nuno Batalha, Ruben Checa, Chantal Lorentz, Pavel Afanasiev, Krzysztof Stańczyk, et al.. Hydrocarbon Fuels from Sequential Hydrothermal Liquefaction (HTL) of Lignite and Catalytic Upgrading of Crude Oil. *Energy & Fuels*, 2024, 38 (2), pp.1019-1031. 10.1021/acs.energyfuels.3c04312 . hal-04433676

**HAL Id: hal-04433676**

**<https://hal.science/hal-04433676v1>**

Submitted on 22 Jul 2024

**HAL** is a multi-disciplinary open access archive for the deposit and dissemination of scientific research documents, whether they are published or not. The documents may come from teaching and research institutions in France or abroad, or from public or private research centers.

L'archive ouverte pluridisciplinaire **HAL**, est destinée au dépôt et à la diffusion de documents scientifiques de niveau recherche, publiés ou non, émanant des établissements d'enseignement et de recherche français ou étrangers, des laboratoires publics ou privés.

1 Hydrocarbon fuels from sequential hydrothermal liquefaction (HTL) of lignite  
2 and catalytic upgrading of crude oil

3  
4 *Nuno Batalha<sup>a\*</sup>, Ruben Checa<sup>a</sup>, Chantal Lorentz<sup>a</sup>, Pavel Afanasiev<sup>a</sup>, Krzysztof Stańczyk<sup>b</sup>, Krzysztof*  
5 *Kapusta<sup>b</sup>, Dorothée Laurenti<sup>a</sup>, Christophe Geantet<sup>a</sup>*

6 <sup>a</sup> Université de Lyon, Institut de Recherches sur la Catalyse et l'Environnement de Lyon (IRCELYON),

7 UMR5256 CNRS-UCB Lyon 1, 2 Avenue Albert Einstein, 69626, Villeurbanne Cedex, France

8 <sup>b</sup> Główny Instytut Górnictwa (Central Mining Institute), Plac Gwarków 1, 40-166 Katowice, Poland

9  
10 \* Corresponding Author: nuno.rocha-batalha@ircelyon.univ-lyon1.fr

11  
12 **ABSTRACT**

13 Lignite from Belchatów in Poland was converted to hydrocarbon fuels, particularly in the kerosene  
14 and diesel range, through sequential hydrothermal liquefaction (HTL) and hydrotreatment (HDT) of  
15 the obtained crude oil. Different HDT temperatures were investigated (from 350°C up to 390°C).  
16 Despite the highly aromatic nature and high heteroatom content, the HTL lignite crude oil could  
17 undergo deep hydrodesulfurization (HDS = 99 %) and hydrodeoxygenation (HDO =98 %) in a single  
18 HDT treatment stage, yielding a liquid product rich in aliphatic and aromatic, particularly  
19 monoaromatic, hydrocarbons. The hydrotreatment and hydrogenating capacity of the lignite crude oil  
20 was linked to the low concentration of compounds resistant to hydrotreatment in lignite and,  
21 consequently, lignite's crude oil, permitting the easy transformation of the crude oil into hydrocarbon  
22 fuel. Still, the significant concentration of aromatic compounds, particularly monoaromatic and  
23 diaromatic, in the liquid product (≈45% of fuel range products) suggests further upgrading, blending,  
24 or harsher HDT conditions might be necessary to improve the fuel quality.

25 In addition to the crude oil, the HTL of lignite yielded a stream of char, which displayed a higher  
26 calorific value and lower heteroatom content than the original lignite feedstock, thus having a high  
27 potential for electricity production, the common use of lignite. Thus, introducing an HTL stage to  
28 extract crude oil before lignite use in electricity production could provide an alternative fuel source  
29 used as a strategy to increase multiple countries' energetic independence.

30 Keywords: Lignite; hydrotreatment; Crude oil; liquid fuels; coal valorization

## 31 1. INTRODUCTION

32 The Russian invasion of Ukraine in February 2022 has redistributed the energetic policy in Europe  
33 (and in the world) and deeply impacted the food and energetic markets and climate issues <sup>1</sup>. For  
34 instance, the European Union (E.U.) is the first market for diesel fuel and must import 20% of its  
35 consumption. Half of this imported diesel was coming from Russia. Despite E.U. policy attempts to  
36 eliminate fossil resources, with a new target of 45% of renewables in 2030, energetic transition and  
37 evolution of energetic policies are challenging to manage, and a portfolio of options must be  
38 investigated. Biofuel production is expected to increase in the future<sup>2</sup>. However, these are only  
39 expected to cover 4.6% of transport fuel demand in 2024<sup>3</sup>. Therefore, there might be a need for a local  
40 diesel resource in the E.U. before vehicles electrification and green fuels are fully implemented.

41 Despite its relatively low heat content, almost 80% of lignite is used for electricity generation<sup>4</sup>.  
42 Even if its production has strongly decreased since the 90's in Europe, the inland consumption of  
43 brown coal by E.U. member states was estimated, in 2021, at 300 Mt <sup>5</sup>. An alternative pathway to  
44 valorize lignite, pure or mixed with waste biomass, is hydrothermal liquefaction. In the absence of  
45 oxygen, subcritical or supercritical water as a reaction medium converts organic matter,  
46 independently of the origin, into a liquid of high heating value (HHV). In early works, Deshpande et al.,  
47 Kershaw et al., and Hu et al. extracted brown coals or Dayan lignites, respectively, with sub and  
48 supercritical water and claimed that the extraction residue would be a good feedstock for combustion  
49 or gazification<sup>6-8</sup>. These studies led to the establishment of the hydrothermal dewatering (HTD)  
50 process, a pretreatment (developed at pilot scale) of lignite with no particular address regarding the  
51 crude oil formed <sup>9</sup>. This was only tackled more recently by Hartman et al., which investigated the HTL  
52 of selected coal feedstocks providing a high liquid yield (21%) and concluded that high-value  
53 petroleum-like products could be obtained <sup>10</sup>. Liu et al. used HTL as a pretreatment before pyrolysis  
54 of Xiaolongtan lignite and suggested three reaction steps discussed hereafter<sup>11</sup>. Like HTL of biomass,  
55 numerous reactions occurring during HTL are favorable for deoxygenation and monomer formation,

56 even if condensation reactions may co-occur. Due to the complexity of the HTL process, the  
57 optimization of operating conditions, i.e., the impact of lignite nature and the understanding of the  
58 formation of the product, have yet to be deeply investigated. Recently, Li et al. attempted to optimize  
59 HTL process parameters for the transformation of demineralized and pretreated lignite, observing  
60 these can impact the liquid yield and composition<sup>12</sup>. They also suggested that HTL promotes the  
61 transfer from polycyclic aromatic hydrocarbons to monocyclic aromatic hydrocarbons. All these  
62 studies indicate that HTL of lignite can potentially provide some fuel. However, no one attempted to  
63 upgrade lignite HTL oil like it was done with the HTL biocrudes of biomass or wastes.

64 In the present work, we investigated the HTL conversion of a Polish lignite and the catalytic upgrading  
65 of the HTL lignite oil obtained. A detailed study of the upgrading operating conditions and their impact  
66 on the nature of the products was performed. After upgrading, a diesel fraction was obtained, showing  
67 that a preliminary HTL stage can provide a fraction of a diesel source and increase the HHV of the  
68 residue used for electricity generation.

69

## 70 **2. EXPERIMENTAL**

### 71 *2.1. Hydrothermal liquefaction of lignite*

72 Lignite from the coal mine of Bełchatów in Poland was used as feedstock. The physicochemical  
73 characteristics of the feedstock are presented in Table 1. The HTL experiments were conducted in a  
74 batch type 1000 ml stainless steel autoclave reactor (Autoclave Engineers, USA), equipped with a  
75 magnetically coupled mechanical stirrer. In each of the HTL experiments, 600 g of 10 wt% of lignite in  
76 water solution was used. After loading the reactor, the residual air was removed by nitrogen purging  
77 and vacuuming four times. Subsequently, the vessel was pressurized with N<sub>2</sub> (~2 bar) and then heated  
78 to 360 °C (reaction temperature) with a constant heating rate 10 °C/min and maintained at this  
79 temperature for 30 min (HTL reaction time). The pressure in the reactor vessel was self-generated.  
80 The experimental conditions used to perform the HTL are summarized in Table 2.

81 After completion of the reaction, the autoclave was cooled to ambient temperature, and the gas  
82 samples were taken for analysis by micro-GC SRA instruments equipped with the following three  
83 modules: MoISieve 5 Å with backflush, PoraPLOT U, and Plot Al<sub>2</sub>O<sub>3</sub>/KCl. The HTL products mixture

84 (crude oil, aqueous phase, and char) were then recovered from the reaction vessel. The separation of  
 85 the products mixture obtained after the HTL processes was performed using a vacuum filtration  
 86 technique. The post-reaction mixture was filtered on glass microfiber filters. The aqueous phase  
 87 obtained was separated from the char. The reactor vessel and the char were washed with acetone,  
 88 and the solid fraction and the liquid organic fraction (crude oil) solution in acetone were separated by  
 89 vacuum filtration. Next, the solid fraction was dried to constant weight in the laboratory drying oven  
 90 at 105 °C. The filtered crude oil solution was concentrated using a rotary vacuum evaporator. The  
 91 scheme of the process is presented in Figure S1.

92 Table 1. Physicochemical properties of lignite feedstock.

Proximate Analysis	Moisture <sub>total</sub> (wt.%) <sup>a</sup>	50.6
	Organic matter (wt.% dry) <sup>b</sup>	72.5
	Volatiles (wt.% dry) <sup>c</sup>	42.0
	Ash (wt.% dry) <sup>d</sup>	25.9
Ultimate analysis	C (wt.% dry)	50.5
	H (wt.% dry)	4.6
	N (wt.% dry)	0.6
	O (wt.% dry)	16.0
	S total (wt.% dry)	3.8
Calorific value <sub>as received</sub> (kJ/kg)		8 130
Calorific value <sub>dry</sub> (kJ/mol)		18 960

93 <sup>a</sup>Weight loss upon heating at 105°C (standard method: CEN/TS 15414-2:2010)

94 <sup>b</sup>Weight loss of dry sample upon combustion under air atmosphere (T = 550 °C). (Standard Method:  
 95 PN-EN 15935:2013-02)

96 <sup>c</sup>Weight loss of dry sample under inert atmosphere (T=950 °C). (standard method: PN-G-04516:1998)

97 <sup>d</sup>Weight remaining after combustion of dry sample under air atmosphere (T=550 °C) (PN-EN  
 98 15935:2013-02)

99

100

101 The yields of the products were calculated based on dry, ash-free (daf) initial lignite using the following  
 102 formulas:

103

$$104 \text{ Crude oil yield (wt. \%)} = \frac{m_{\text{crude}}}{m_{\text{lignite}}} 100$$

Equation 1

105

106  $Char\ yield\ (wt.\ \%) = \frac{m_{char}}{m_{lignite}} 100$  Equation 2

107  $Gas\ yield\ (wt.\ \%) = \frac{\sum^i M_{w_i} y_i P V}{R T m_{Lignite}} 100$  Equation 3

108  $Aqueous\ phase\ solubles\ yield\ (wt.\ \%) = 100 - gas\ yield - char\ yield - crude\ oil\ yield$   
 109 Equation 4

110

111 Where:

112  $m_{crude}$ ,  $m_{char}$ , and  $m_{lignite}$  are the mass of recovered crude oil, recovered char, and initial lignite feedstock  
 113 on a dry, ash-free (daf) basis;

114  $M_{w_i}$  and  $y_i$  are the molecular weight and gas composition of compound  $i$ , respectively.

115  $P$  is the residual reactor pressure at room temperature

116  $V$  is the reactor volume occupied by gas (400 mL)

117  $R$ , is the ideal gas constant

118  $T$ , is the room temperature

119

120

121 Table 2. Summary of experimental conditions used for the hydrothermal liquefaction and  
 122 hydrotreatment test.

Hydrothermal liquefaction (HTL)	
Feedstock	Lignite (Bełchatów, Poland)
Slurry concentration (wt.%)	10 (in water)
Batch volume (L)	0.6
Temperature (°C)	360
Reaction time (h)	0.5
Hydrotreatment (HDT)	
Feedstock	Lignite HTL crude oil
Feedstock mass (g)	3
Catalyst	NiMoS/P-Al <sub>2</sub> O <sub>3</sub>
Catalyst mass (g)	1
Solvent	n-heptane
Solvent mass (g)	25
Reaction temperature (°C)	350, 375 and 390
Reaction time (h)	0, 1, and 3
Hydrogen pressure (bar)	10 (at room temperature) + 50 (at reaction temperature)

123



147 After the reaction, the reactor was cooled to room temperature, and the residual gas was collected in  
 148 a gas bag and analyzed with a micro-GC (SRA instruments) equipped with three modules: Molsieve 5Å  
 149 (H<sub>2</sub>, CO, CH<sub>4</sub>), Hayesep A (CO<sub>2</sub>, C<sub>2</sub> hydrocarbons), PLOT Al<sub>2</sub>O<sub>3</sub>/KCl (C<sub>3</sub>-C<sub>4</sub> hydrocarbons).

150 The liquid and all solids were separated through filtration and washing with heptane (≈ 100 mL). The  
 151 heptane in the liquid was evaporated, using a rotovapor apparatus, for 2 h at a pressure of 30 mBar  
 152 and a temperature of 40°C. The liquid remaining after evaporation was considered the liquid product  
 153 from hydrotreatment. The solids recovered from filtration were dried at room temperature under a  
 154 fumehood to remove the excess heptane. The total amount of solids produced in the reaction resulted  
 155 from the difference between the dried solids and the fresh catalyst. Elemental analysis was used to  
 156 determine the coke deposited in the catalyst, i.e., coke equivalent to carbon in the spent catalyst.

157 The yields of the products obtained from the hydrotreatment (HDT) reaction, i.e., liquid, solid, gas,  
 158 H<sub>2</sub>O, and H<sub>2</sub>S were calculated through the following equations:

159  
 160 
$$\text{Liquid yield (wt. \%)} = \frac{m_{\text{liquid}}}{m_{\text{crude oil}}} 100 \quad \text{Equation 6}$$

161  
 162 
$$\text{solid yield (wt. \%)} = \frac{m_{\text{solid}}}{m_{\text{crude oil}}} 100 \quad \text{Equation 7}$$

163 
$$\text{Gas yield (wt. \%)} = \frac{\sum^i M w_i y_i P V}{R T m_{\text{crude oil}}} 100 \quad \text{Equation 8}$$

164 
$$H_2O \text{ (wt. \%)} = (O_{\text{crude oil}} - \text{Gas yield} \left( \frac{\%CO}{28} + 2 \frac{\%CO_2}{44} \right) 16 - \text{Liquid yield} \cdot O_{\text{liquid}}) \frac{18}{16} \quad \text{Equation 9}$$

165 
$$H_2S \text{ (wt. \%)} = (S_{\text{crude oil}} - \text{Liquid yield} \cdot S_{\text{liquid}}) \frac{34}{32} \quad \text{Equation 10}$$

166  
 167 Where:  
 168  $m_{\text{crude oil}}$ ,  $m_{\text{solid}}$ , and  $m_{\text{liquid}}$  are, respectively, the mass of crude oil to be hydrotreated, the excess of  
 169 mass found in the catalyst after reaction ( $m_{\text{spent catalyst}} - m_{\text{fresh catalyst}}$ ), and the mass liquid obtained after  
 170 evaporation of n-heptane;  
 171  $M w_i$  and  $y_i$  are the molecular weight and gas composition of compound i, respectively.  
 172 P is the residual reactor pressure at room temperature  
 173 V is the reactor volume occupied by gas (≈ 263 mL)  
 174 R, is the ideal gas constant  
 175 T, is the room temperature



176 O, is the weight fraction of oxygen in the crude oil ( $O_{\text{crude oil}}$ ) and liquid ( $O_{\text{liquid}}$ ) determined by elemental  
177 analysis.  
178 %CO and %CO<sub>2</sub>, are the weight fraction of CO and CO<sub>2</sub>, respectively, in the gas  
179 S, is the weight fraction of Sulfur in the crude oil ( $S_{\text{crude oil}}$ ) and liquid ( $S_{\text{liquid}}$ ).

180

### 181 2.3. Characterization methods

182 Elemental compositions (CHNS) of lignite, crude oil, hydrotreatment liquid, and spent catalyst were  
183 analyzed on a Thermo Scientific FLASH 2000 Organic Elemental Analyzer (accuracy of  $\pm 0.1$  wt%). The  
184 samples' oxygen (O) composition was also determined by elemental analysis with the same equipment  
185 used for CHNS quantification but by using an alternative method specifically dedicated to oxygen  
186 quantification. Additionally, the S composition of the crude oil and hydrotreatment liquid samples  
187 were also quantified using ANTEK 9000NS apparatus, which is more sensitive (from few ppm until  
188 percent levels) and accurate. Prior to analysis, the samples were diluted in THF ( $\approx 5$  wt%).

189 The boiling point of the sulfur-containing compounds in the crude oil was estimated by using a Agilent  
190 7890A GC coupled with an FPD+ detector and fitted with a CP-SimDist GC column (10 m  $\times$  0.53mm  $\times$   
191 2.65  $\mu$ m).

192 The molecular weight distribution of the compounds in the lignite crude oil and the hydrotreatment  
193 liquid was obtained by size exclusion chromatography (SEC) performed using an Agilent 1200 series  
194 HPLC equipped with two PLgel Columns (50 and 500  $\text{\AA}$ ), a refractive index detector (RID), and a diode  
195 array detector (DAD). The analysis was carried out at 35  $^{\circ}$ C using tetrahydrofuran (THF – 1 mL/min) as  
196 the eluent. Before analysis, the samples were diluted to a concentration of  $\approx 1$  wt.% in THF and filtered  
197 (0.45  $\mu$ m). A mixture composed of hydrocarbons (Mw from 86 to 1000 g/mol) was used as standard  
198 to convert elution time into molecular weight (hydrocarbons equivalent) leading to an average  $MW_{\text{HC}}$   
199 data.

200 The <sup>13</sup>C-NMR analysis of the liquid samples was performed in a Bruker AVANCE 400 MHz spectrometer  
201 and analyzed using the software TopSpin 3.0. The measurements were performed at room  
202 temperature with an accumulation of 4700 scans, with a relaxation time of 10 s, for approximately 15  
203 h. The samples ( $\approx 100$  mg) were diluted with deuterated chloroform (CDCl<sub>3</sub>) (0.6 mL). Table S2 includes  
204 the chemical shifts attributed to each functional group.

205 Comprehensive GC $\times$ GC-TOF MS and GC $\times$ GC-FID were used to identify and quantify the compounds in  
206 the lignite crude oil and HDT liquid. The GC $\times$ GC/TOF system was equipped with a cryogenic modulator

207 from Zoex Corporation (USA) and a BenchTOF 2 TI spectrometer from Sepsolve. The chromatograph  
208 and TOF parameters are described in Tables S3 and S4. The GC×GC/FID was equipped with a switch  
209 valve modulator (Agilent G3486A CFT modulator), and modulation parameters were optimized  
210 according to ref <sup>13</sup>. The parameters used for product separation are described in Table S3. The  
211 quantification of the compounds detected by GC×GC-FID was performed using the relative responsive  
212 factor method (RRF)<sup>14</sup> with cyclohexanol as the reference. The data obtained from comprehensive  
213 GC×GC-FID was also used to provide the distillation curve of the HDT liquid products by using a mixture  
214 of n-alkanes (C<sub>7</sub> to C<sub>40</sub>) as a reference.

215

### 216 **3. RESULTS AND DISCUSSION**

#### 217 ***3.1. Hydrothermal liquefaction of lignite***

##### 218 ***3.1.1. Crude oil***

219 While the primary target product for liquid fuel production is crude oil, only 12.3 wt.%daf of lignite  
220 was transformed into this product with char (48.8 wt.%daf), gas (23wt.% daf), and aqueous phase  
221 organics (15.9 wt.%daf) representing the main fractions. Liu et al. <sup>15</sup> studied the optimal conditions for  
222 maximizing crude oil yield from lignite HTL and found that short residence times, i.e., ~5 min, and high  
223 temperatures, i.e., ~400 °C, are necessary. In this study<sup>15</sup>, the authors found a maximum crude yield  
224 of 34 wt.%. Hence, the high residence time (30 min) and low temperature (360 °C) presently used can  
225 explain the low crude oil yield. Another important parameter known to affect the yield and quality of  
226 crude oil in HTL is the amount of ash <sup>16–20</sup>. On biogenic feedstocks, such as algae, high ash contents  
227 have been reported to decrease the yield and quality of the crude product <sup>16–18</sup>. Although no reference  
228 applied to the conversion of lignite under HTL conditions was found, a direct analogy with biomass  
229 feedstocks suggests that high-ash in lignite might have a similar effect. Thus, a high concentration of  
230 ash found in lignite (25.94 wt.%) could also be responsible for the low crude oil yield (12.3 wt.%).  
231 Indeed, Liu et al. <sup>15</sup> used lignite with 7.14 wt.% of ash. It should be mentioned that Oner et al.  
232 demonstrated that ash positively enhances the crude oil product in lignite liquefaction under organic  
233 solvents, like tetraline, and under H<sub>2</sub> pressure <sup>21</sup>. However, the positive effects were attributed to the

234 capacity of certain elements in ash to promote hydrogenation by H<sub>2</sub> or hydrogen transfer from the  
235 solvent, a reaction not likely to occur under HTL conditions. While ash is bound to affect lignite HTL  
236 conversion, the chemical composition of lignite and lignite's ash is substantially different from that of  
237 biomass feedstocks<sup>22,23</sup>. Thus, further studies, out of the scope of this work, should be performed to  
238 infer the impact of this component.

239 When compared to the lignite feedstock, the crude oil stream contains a higher concentration of  
240 carbon (77.7 wt.% vs. 50.5 wt.%dry) and hydrogen (8.9 wt.% vs.4.6 wt.%dry) (Tables 1 and 2).  
241 Additionally, the crude oil displayed a lower concentration of oxygen (10.8 wt.% vs. 16.0 wt.%dry) and  
242 sulfur (2.4 wt.% vs. 3.78 wt.%dry) than the parent lignite sample. However, it is essential to mention  
243 that the sulfur content in crude oil is still well above the specifications for liquid hydrocarbon fuels,  
244 e.g., diesel specification < 10 ppm. Thus, significant desulfurization must take place during upgrading.  
245 In the case of nitrogen, no specification states a maximum N concentration in hydrocarbon fossil  
246 fuels<sup>24</sup>. Still, nitrogen compounds impact other regulated properties, such as gum content, storage  
247 stability, and thermal stability<sup>25</sup>. However, synthetic aviation fuels (SAF) must have a nitrogen  
248 concentration inferior to 2 ppm<sup>26</sup>. It is worth mentioning that there is still no regulation concerning  
249 HTL-derived fuels.

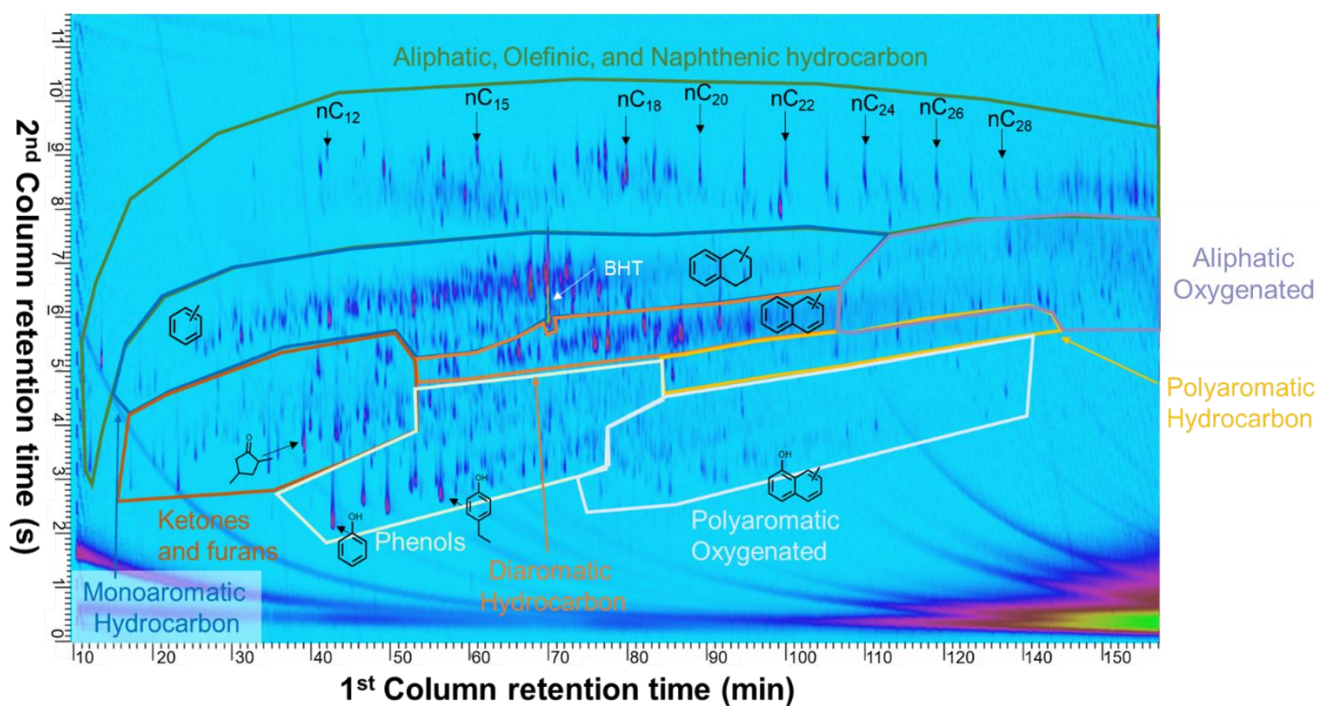
250 The functional group's composition, determined by <sup>13</sup>C NMR, of the crude oil is shown in Table 3. The  
251 crude oil is mainly composed of aliphatic (53.6%) and aromatic (40.3%) carbon. Among the aromatic  
252 carbon, 24.0% corresponded to C-H bonds, 9.6% to C-C bonds, and 6.8% to C-O bonds (chemical shift  
253 and NMR Spectrum in Table S2 and Figure S2, respectively). Alkyl groups or polyaromatics compounds  
254 in crude oil can explain the occurrence of C-C bonds in aromatic fraction. Additionally, the high  
255 incidence of aromatic C-O and carbonyl C=O, compared to the methoxy, aliphatic, carboxylic acid, and  
256 esters, indicates that phenolic compounds and ketones represent a significant portion of the crude oil  
257 oxygen. Indeed, the crude oil composition analysis by comprehensive GC×GC-TOFMS (Figure 1)  
258 showed the presence of ketones, furans, phenols, and naphthols. A small amount of mono-aromatic

259 and di-aromatic hydrocarbons and non-aromatic cyclic hydrocarbons, possibly derived from  
 260 biomarkers typically present in lignites<sup>27</sup>, were also found. The quantification performed by GCxGC-  
 261 FID is shown in Table 4. Only 16.7 wt.% of the crude oil sample was detectable by GCxGC-FID analysis.  
 262 The non-detected compounds were too heavy to be analyzed by gas chromatography. Indeed, Liu et  
 263 al. analyzed the heteroatom-containing compounds obtained from the ethanolysis of lignite via  
 264 Fourier transform ion cyclotron resonance mass spectroscopy (FTICR-MS), observing a significant  
 265 number of oxygenated compounds with up to 6 aromatic rings with the particular occurrence of  
 266 oxygenated molecules with carbon number between 17 and 26 carbons and two oxygen atoms, like  
 267 organic acids and diols<sup>28</sup>. In the same study, authors characterized the sulfur-containing compounds,  
 268 mostly ranging above C<sub>20</sub> and associated in the same molecule with another S or several O atoms.<sup>28</sup>  
 269 The relatively large carbon number of the sulfur-containing compounds in crude oil can explain the  
 270 few S compounds detected in the products by comprehensive GCxGC-TOFMS (Figure 1). Indeed, the  
 271 analysis of the sulfur content of the crude oil sample by GC-FPD<sup>+</sup> using a Simdis chromatography  
 272 method equivalent to ASTM D2887 reveals that such molecules have a retention time higher than  
 273 hexatriacontane (C<sub>36</sub> - Bp = 497 °C) (Figure S3), which defines the upper detection limit of the GCxGC  
 274 analysis. The same explanation can be given for the few nitrogen-containing compounds among the  
 275 GCxGC detected compounds in the crude oil (Figure 1).

276 Table 3. Composition of crude oil obtained from the HTL of Bełchatów lignite

Composition		Carbon chemical composition ( <sup>13</sup> C NMR) <sup>a</sup>	
C (wt.%)	77.7 ± 0.1	C <sub>Aliphatic</sub>	53.6
H (wt.)	8.9 ± 0.3	C <sub>Methoxy</sub> (-O-CH <sub>3</sub> )	0.1
O (wt.%)	10.8 ± 1.0	C <sub>Aliphatic-O</sub> (-O-(CH <sub>2</sub> ) <sub>n</sub> )	0.8
S (ppm)	2.4 ± 0.1	C <sub>Aromatic</sub>	40.3
N (ppm)	0.5 ± 0.1	C <sub>Carboxylic/Amide</sub>	0.8
TAN (mg <sub>KOH</sub> /g)	29.2 ± 0.2	C <sub>Aldehyde/Ketone</sub>	4.4
HHV (MJ/kg)	31.8		

277 <sup>a</sup>Chemical shift range in Table S1 and NMR spectra in Figure S2



278

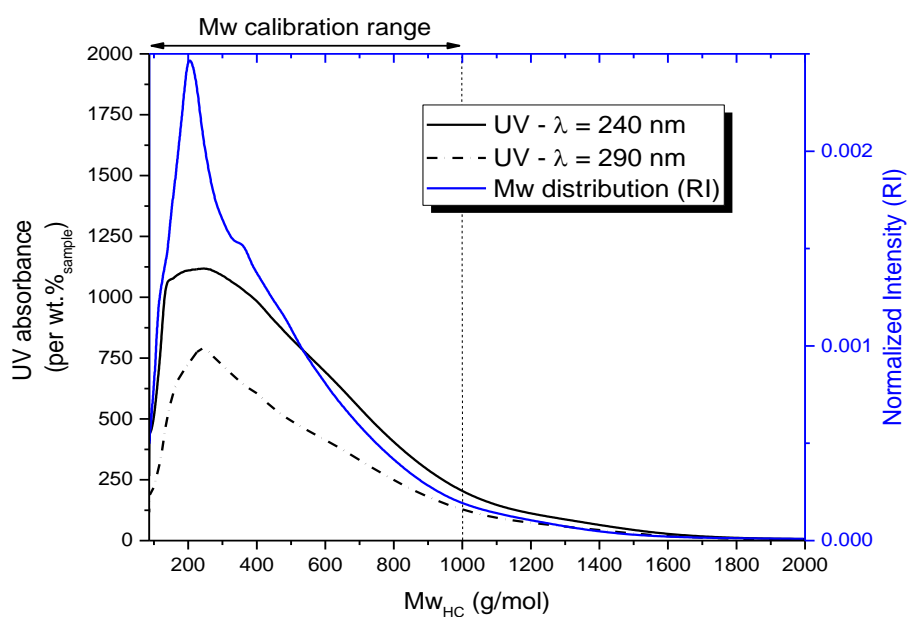
279 Figure 1. GCxGC-TOF MS chromatogram of the crude oil obtained from the HTL of lignite. BHT  
 280 (butylated hydroxytoluene) originates from THF solvent, where it serves as a stabilizer.

281

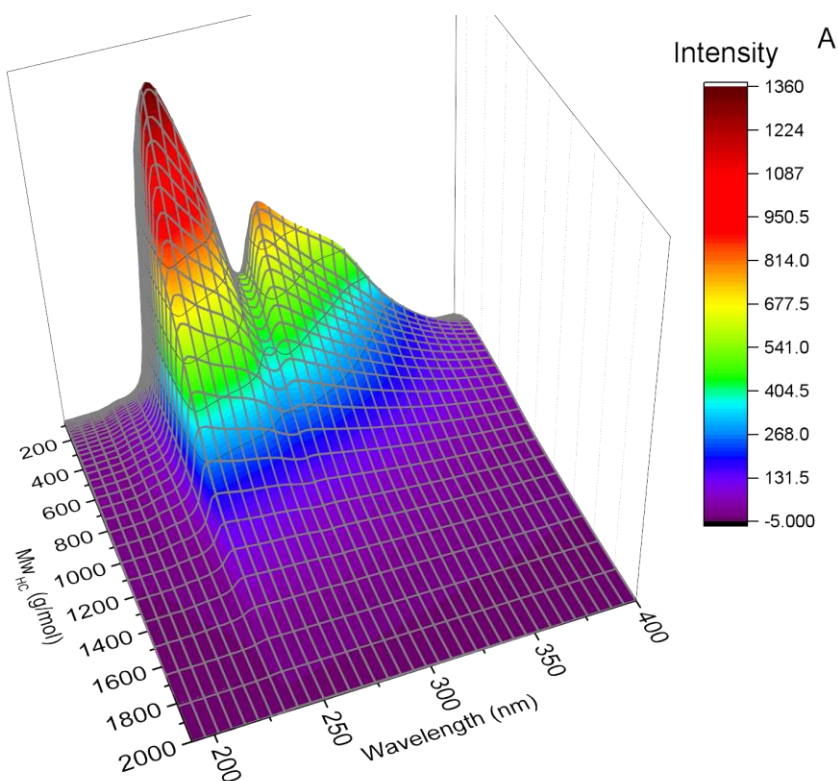
282 Table 4. Quantification of the lignite HTL oil compounds detected by GCxGC-FID using the relative  
 283 response factor method (supporting information). The chromatogram and the areas attributed to  
 284 each compound family are represented in Figure 1.

Compounds	Oil composition (wt.%)	Compounds	Oil composition (wt.%)
Aliphatic HC	1.6	Ketones and furans	0.6
Monoaromatic HC	1.6	Phenols	1.4
Diaromatic HC	1.6	Polyaromatic Oxygenated	2.2
Polyaromatic HC	1.2	Aliphatic Oxygenated	6.5

285



286



287

288 **Figure 2.** A) Compounds in the liquid product molecular weight ( $Mw_{HC}$ ) distribution determined by  
 289 refraction index (RI) (blue curve) and UV absorbance ( $\lambda = 240$  nm and 290 nm) as a function of the  
 290 compounds Mw. Average Mw = 297 g/mol. B) DAD spectrum ( $\lambda = 190 - 400$  nm) of crude oil as a  
 291 function of molecular weight ( $Mw_{HC}$ ).

292

293 A better insight into heavy molecules is given by SEC. The molecular weight distribution of the crude  
294 oil components (Figure 2-A) reveals a large range of compounds, with a molecular weight of up to  
295 ~1,800 g/mol in HC eq. and an average molecular weight of 297 g/mol in HC eq. The significant  
296 presence of large Mw molecules, which are expected to have a high boiling point, agrees with the  
297 small detection level observed in the GCxGC analysis. The evolution of the DAD spectra as a function  
298 of molecular weight (Figure 2-B) reveals an intense absorption between 240 and 400 nm, reflecting  
299 the high aromatic nature of the compounds in the crude oil. The presence of two absorption  
300 maximums, 245 nm and 293, and a shoulder at 316 nm indicates that polyaromatic compounds are  
301 abundant in the crude oil sample. Indeed, as exemplified in Figure S4, monoaromatic compounds like  
302 benzene generate a DAD band at ~250 nm. In opposition, polyaromatic compounds with two or more  
303 conjugated aromatic rings present a second absorption band at  $\lambda > 290$  nm (Figures S5, S6, and S7). In  
304 the particular case of naphthalene, a second sharp peak was observed at 290 nm, with identical  
305 intensity to the peak centered at 250 nm (Figure S5), while in anthracene and pyrene, this band is  
306 significantly broader, extending to significantly higher  $\lambda$  (Figures S6 and S7). Therefore, in the crude  
307 oil (Figure 2-A), the wide absorption band at  $250 > \lambda > 400$  nm indicates the presence of compounds  
308 with at least 3 and 4 conjugated aromatic rings.

309 The comparison of the Mw distribution and the UV absorbance at  $\lambda=240$  nm and 290 nm as a function  
310 of the Mw reveals that both RI and UV curves have a maximum at Mw ~ 230 g/mol (Figure 2-A).  
311 However, the UV spectra absorption distribution is shifted to higher Mw, evidencing heavier  
312 molecules with high aromaticity.

313

### 314 **3.1.2. Char, gas, and aqueous phase**

315 The hydrothermal liquefaction of lignite (soft Miocene lignite) obtained in the Bełchatów coal mine in  
316 Poland led to four product streams, i.e., gas, char, crude oil, and an aqueous phase rich in organic  
317 matter. Char was the most abundant among the product streams, representing 48.8 wt.% of the lignite

318 feedstock yield. Even though char and lignite are both solids, the former displayed a higher carbon  
319 content with lower oxygen, nitrogen, hydrogen, and sulfur (Table S4). Hence, char displayed O/C and  
320 H/C ratios of 0.1 and 0.4, respectively, while lignite O/C was 0.2 and H/C was 1.1. The different solid  
321 composition explains char's slightly higher heating value compared with the lignite feedstock, i.e., 22.6  
322 MJ/kg<sub>Dry</sub> vs. 19.0 MJ/kg<sub>Dry</sub>, respectively. P. Liu and D. Zhang<sup>29</sup> studied the transformation of lignite  
323 under hydrothermal conditions, observing that, at T=260 °C, significant removals of oxygen and  
324 hydrogen occur. Similar observations were made by Z. Shi et al.<sup>30</sup>, who, like P. Liu and D. Zhang,  
325 observed a significant reduction of carboxyl, carbonyl, and oxygenated aliphatic carbon in the solid  
326 after HTL treatment. These authors also observed a reduction of the aliphatic CH<sub>2</sub> and CH<sub>3</sub> groups after  
327 hydrothermal treatment, which justifies the decrease in the H/C ratio. The authors linked the  
328 elimination of oxygen and hydrogen from the lignite structure to the production of light gases, such  
329 as CO, CO<sub>2</sub>, and light hydrocarbons<sup>29,30</sup>. Like O and H, the sulfur in char was significantly smaller than  
330 in the lignite feedstock, i.e., 1.1 wt.% vs. 3.78 wt.%, respectively, indicating only 14.2 % of sulfur  
331 remained in the solid phase after hydrothermal liquefaction. The significant extent of desulfurization  
332 is directly related to the nature of the sulfur compounds in lignite. As low-ranking coals, lignites  
333 contain more substantial amounts of sulfides and thiols than other types of coal<sup>31</sup>, which are more  
334 easily transformed under hydrothermal conditions<sup>32,33</sup>.

335 The lower impurities content, i.e., O, N, and S, and increased calorific value indicate that char is a  
336 higher quality coal than the original lignite. Indeed, the treatment of coal samples through  
337 hydrothermal liquefaction has been demonstrated to increase the quality of coal samples, both by  
338 eliminating impurities and improving hydrophobicity<sup>12,30,34,35</sup>.

339 The composition of the gas stream formed during the hydrothermal liquefaction of lignite is shown in  
340 Table S5. CO<sub>2</sub> was the majority product in the gas phase, corresponding to 92.6 wt.% of all the  
341 produced gases. The high CO<sub>2</sub> selectivity in the gas products obtained from lignite HTL had already  
342 been reported previously<sup>15,30</sup>, indicating that decarboxylation is one of the primary processes  
343 responsible for oxygen removal during the reaction. Indeed, CO only represented 1.4 wt.% of the



344 gases, suggesting decarbonylation is significantly less favored. H<sub>2</sub>S represents the second most  
345 abundant compound in the gas stream, representing 3.4 wt.% of all gases. Furthermore, 19.4% of the  
346 sulfur in the lignite feedstock was transformed into H<sub>2</sub>S. The significant formation of H<sub>2</sub>S reflects the  
347 transformation of organic, i.e., thiol and sulfide, and inorganic sulfur, i.e., pyrite, compounds in lignite  
348 promoted by H radicals under hydrothermal conditions<sup>32,33,36</sup>. In addition to CO<sub>2</sub>, CO, and H<sub>2</sub>S, small  
349 amounts of light hydrocarbons and H<sub>2</sub> (Table S5) were also observed. Nonetheless, the amount of such  
350 compounds is not enough to justify alone the small H/C observed in the char, thus suggesting that  
351 light hydrocarbons and H<sub>2</sub> formation are not the main ones responsible for the elimination of  
352 hydrogen in the lignite as proposed by Z. Shi et al., and P. Liu and D. Zhang<sup>29,30</sup>. Instead, the  
353 transformation of lighter fractions of lignite into aqueous and crude organic compounds is more likely  
354 to cause the low H/C of char compared to lignite.

355 Finally, the organic matter solubilized in the aqueous reaction media, i.e., the aqueous phase,  
356 represented 15.9 wt.% of feedstock lignite. In hydrothermal liquefaction processes, the aqueous  
357 phase is typically composed of organic acids, e.g., acetic acid, oxygenated aromatics, aromatic, like  
358 phenols, nitrogenated compounds, and oxidized sulfur compounds<sup>33,37,38</sup>, thus justifying this stream's  
359 acidic pH of 5.2.

360

### 361 **3.2. Hydrotreatment of lignite HTL crude oil**

362 The significant concentration of heteroatoms and polyaromatic compounds in the crude oil stream  
363 clearly demonstrates the necessity of further upgrading for the production of hydrocarbon fuels.  
364 Therefore, this section will focus on the hydrotreatment of the crude oil stream obtained from the  
365 hydrothermal liquefaction of lignite. The hydrotreatment of the lignite crude oil was performed at  
366 three different temperatures, i.e., 350 °C, 375 °C, and 390°C, and at two different reaction times, 1 h  
367 and 3 h. An additional residence time, where the reaction was stopped after the reaction temperature  
368 was attained ( $t_{\text{heating}} = 20 \text{ min}$ ), designated  $t = 0 \text{ h}$ , was also performed at each temperature. The crude

369 oil conversion occurring before  $t = 0$  h are caused primarily by thermal processes. For each operating  
370 condition, five product streams (Figure 3-A) were obtained, i.e., gas, liquid, solid, and  $H_2S$  and  $H_2O$   
371 estimated using equations 9 and 10.

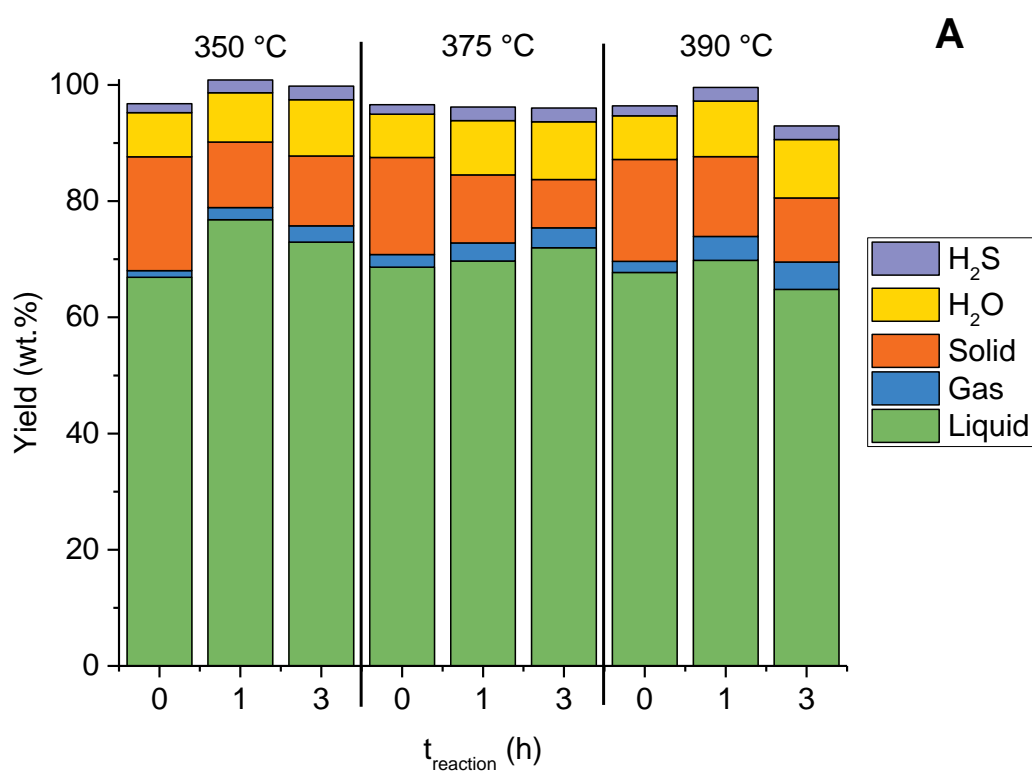
### 372 **3.2.1. Solid product**

373 The solid product was found to decrease as a function of the reaction time. Indeed, for the  $t = 0$  h  
374 experiments, the solid fraction yield was  $\approx 16.7 - 19.6$ wt.%, while the solid yield decreased to  $\approx 9 - 12$   
375 wt.% for longer residence time. It should be mentioned that no solid products, such as char, other  
376 than the spent catalyst, could be visually observed after the reaction. Consequently, at least part of  
377 the solid product is represented by heavy asphaltene-like products that can be converted under the  
378 reaction conditions but are not soluble in heptane and stay with the catalyst after the reaction. Table  
379 S6 contains the carbon loading of the spent catalyst after the reaction, showing that higher reaction  
380 time and temperatures lead to lower carbon deposition on the catalyst's surface. Furthermore, at the  
381 temperature of  $375^\circ C$  and  $390^\circ C$  after 3 h, the carbon deposition on the spent catalyst was  $\approx 5$  wt.%,  
382 which is compatible with the typical coke loadings observed in the early stages of operating HDT  
383 catalysts<sup>39</sup>. Hence, the crude oil feedstock did not lead to enhanced deactivation by coke deposition  
384 of the sulfided catalyst, as observed for HTL crude oils from other sources, like sewage sludge<sup>40</sup>.

### 385 **3.2.2. Gas product**

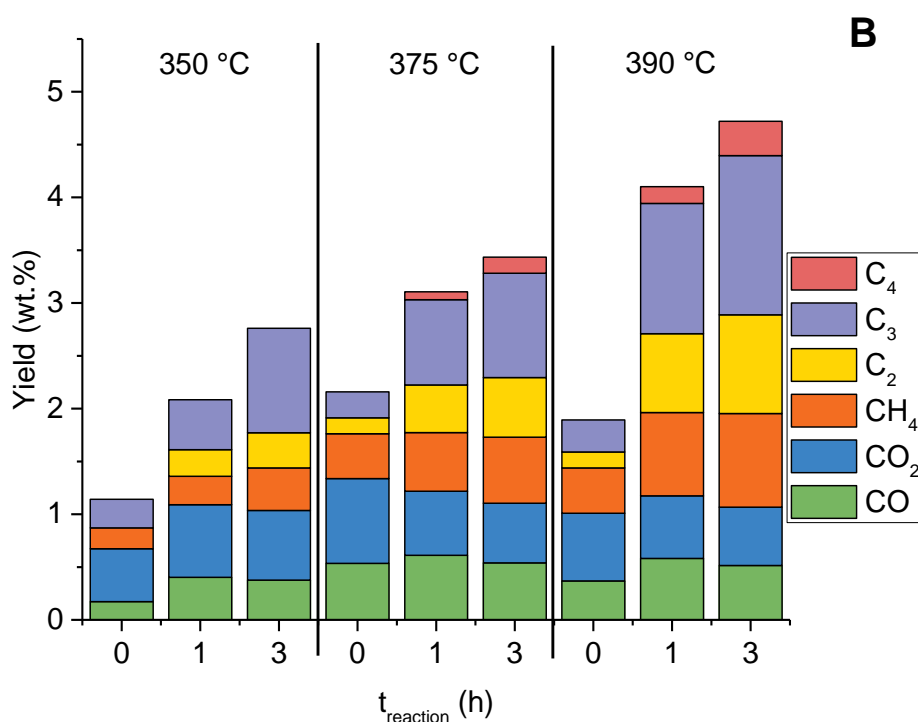
386 The yield and composition of the gas products are shown in Figure 3-B. In general, the yield of gas  
387 increases with the reaction temperature and reaction time, achieving a maximum of 4.7 wt.% for the  
388 reaction conditions of  $390^\circ C$  and 3 h. Still, the yield of gas products like CO and  $CO_2$ , which result from  
389 decarboxylation and decarbonylation reactions, was found to stay constant, between 0.4-0.6 wt.%  
390 and 0.6 – 0.8 wt.%, respectively, after 1 h of reaction independently of the temperature (Figure 3-B).  
391 The low yield of CO and  $CO_2$  is attributed to the minor contribution of aliphatic C-O, methoxy, and acid  
392 groups in the crude oil (Table 3). Indeed, the oxygen in the crude oil was primarily eliminated as  $H_2O$ ,  
393 whose yield is between 7.5 wt.% and 10.0 wt.%. Light hydrocarbons, like  $CH_4$ ,  $C_2H_6$  ( $C_2$ ),  $C_3H_8$  ( $C_3$ ), and

394 C<sub>4</sub>H<sub>10</sub> (C<sub>4</sub>), were the main compounds responsible for the gas yield increase observed at higher  
 395 temperature and reaction time (Figure 3-B). While the formation of light hydrocarbons can be  
 396 explained by C-C bond cleavage caused by hydrogenolysis, which is favored at higher temperatures,  
 397 heptane cracking does not seem to contribute significantly to the gas products since the  $\frac{C_3}{C_4}$  ratio is  
 398 significantly higher than 1 (Figure 3-B). Indeed, on sulfided catalysts, like NiMoS/P-Al<sub>2</sub>O<sub>3</sub>, heptane  
 399 hydroconversion occurs preferably through  $\beta$ -scission, yet this mechanism only becomes relevant at  
 400 temperatures above the ones used in this study, i.e., T > 400 °C<sup>41,42</sup>. Instead, light hydrocarbons most  
 401 likely result from the cleavage of larger molecules from the crude oil during the hydrotreatment  
 402 reaction.



403

404



405

406 Figure 3. A) Product yields, determined according to equations 6 to 10, obtained from the HDT of the  
 407 lignite HTL crude oil. B) Gas products yield as a function of reaction temperature and time, obtained  
 408 from the HDT of the lignite HTL crude oil.

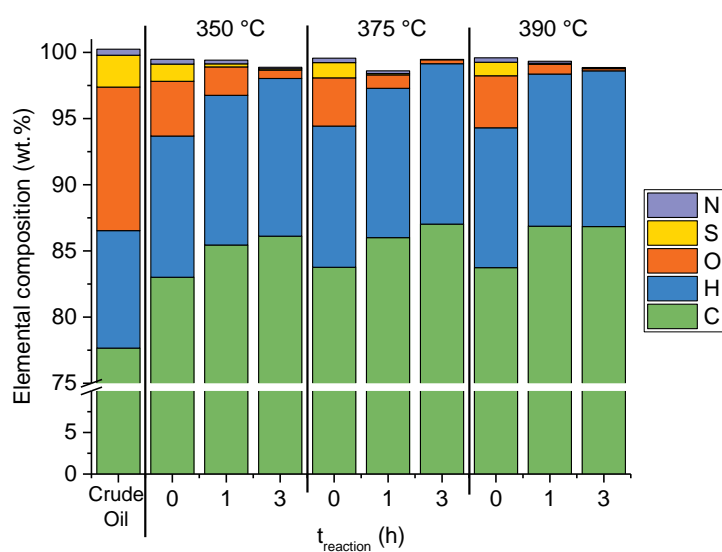
409

### 410 3.2.3. Liquid product

411 After upgrading, the liquid product yield varied between 65 wt.% and 77 wt.% depending on the  
 412 reaction temperature and time (Figure 3-A). In all cases, the liquid yield was slightly higher after 1 h of  
 413 reaction as compared to  $t_{\text{reaction}} = 0$  h, which agrees with the hypothesis previously stated on the  
 414 conversion of solid products existing at the early stages of the reaction (section 3.2.1). After 3h of  
 415 reaction, the liquid produced stabilized at 375 °C or slightly decreased at 350 °C and 390 °C due to the  
 416 lower amount of solid converted in this time (Figure 3-A and Table S6) and the HDT reactions.

417 The elemental composition of the HDT liquid product is shown in Figure 4. When compared with the  
 418 crude oil feedstock (Table 3), the HDT liquid products contained a higher concentration of carbon and  
 419 hydrogen (Figure 4) even at  $t_{\text{reaction}} = 0$  h. Similarly, the concentration of heteroatoms in the liquid  
 420 product was also significantly smaller at  $t_{\text{reaction}} = 0$  h than on the parent crude oil sample, with

421 deoxygenation, denitrogenation, and desulfurization in the range of 60%, 30% and 50% respectively  
 422 (Tables S7 to S9). It should be mentioned during heating, H<sub>2</sub> pressure is reduced (10 bar, at room  
 423 temperature) and that heating up to the reaction temperature takes 20 min. Thus, the significant  
 424 elimination of heteroatoms during heating suggests these be easily removable under relatively mild  
 425 conditions or by thermal degradation. Furthermore, HDO, HDS, and, to a lesser extent, HDN (Tables  
 426 S7 to S9) significantly increased with the reaction time, reaching above 94 %, 96 %, and 78%,  
 427 respectively, after 3 h of reaction. On the other hand, high denitrogenation levels required a higher  
 428 temperature, such as 390 °C, with the HDN rate being significantly favored at higher temperatures.  
 429 The efficient removal of heteroatoms suggests that the hetero-compounds in the crude oil feedstock  
 430 are not in the form of refractory compounds, i.e., polyaromatic sulfur and nitrogen compounds<sup>43,44</sup>, as  
 431 indicated by Liu et al.<sup>28</sup>. It is relevant to mention that most HTL crude oils from bio-sourced feedstocks,  
 432 like algae, food waste, and sewage sludge, require two stages of upgrading to remove heteroatoms  
 433 effectively<sup>37,45,46</sup>. Yet, nearly all lignite crude oil's sulfur, nitrogen, and oxygen were removed after a  
 434 single hydrotreatment step on NiMoS/P-Al<sub>2</sub>O<sub>3</sub> catalyst. Still, in the best-case scenario, 30 ppm of sulfur  
 435 was found in the liquid, indicating further desulfurization via a second HDT stage, harsher conditions,  
 436 or blending is necessary to meet the minimum requirements of a drop-in fuel from lignite crude oil.



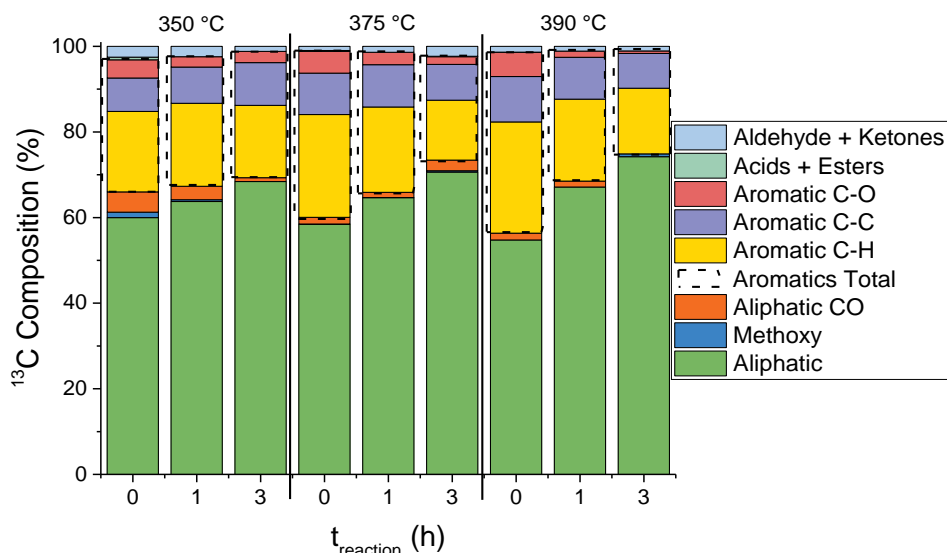
437

438 Figure 4. Elemental analysis of lignite crude oil and the liquid product obtained from HDT of lignite  
439 crude oil at different reaction temperatures (350 °C, 375 °C, and 390 °C) and reaction times ( $t_{\text{reaction}}$ ).

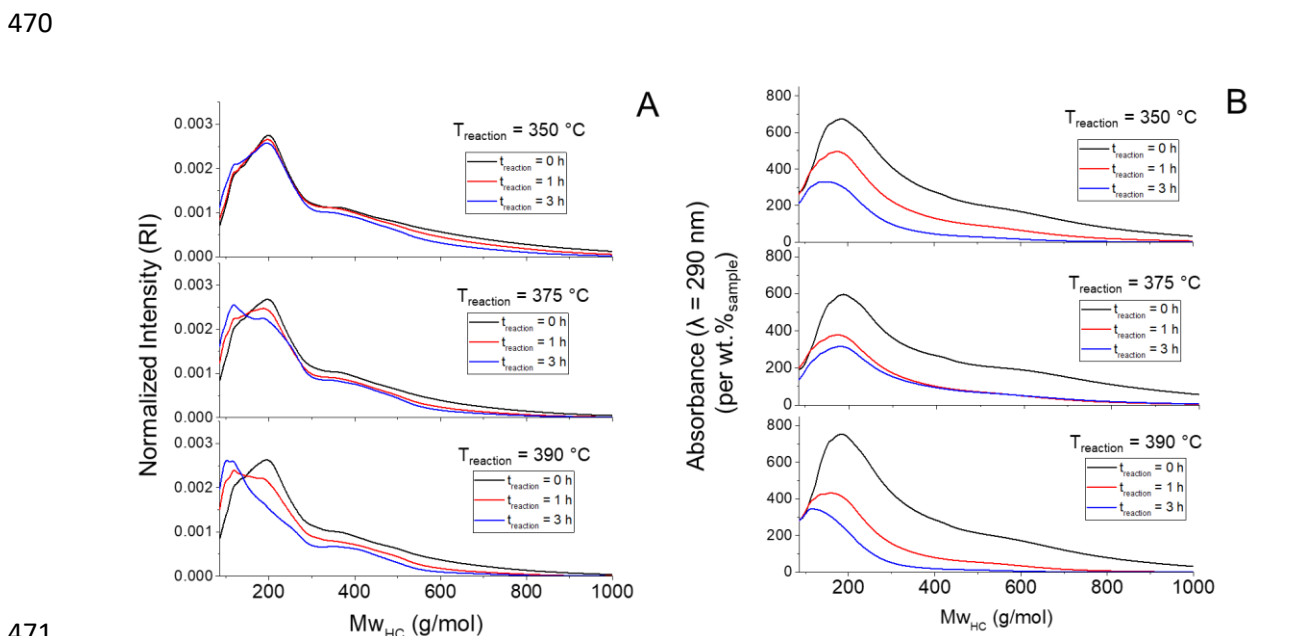
440

441 The evolution of the functional groups upon HDT, determined by  $^{13}\text{C}$  NMR, is shown in Figure 5. In  
442 comparison with the crude oil, the distribution of the functional groups of the liquid product clearly  
443 shows a significant increase in the aliphatic carbon, i.e., from 40.1%, in crude oil, to 54.8 – 74.2% in  
444 the liquid, accompanied by a reduction of the aromatic carbon, i.e., 54.3% to 42.3 – 24.0%. When  
445 comparing the HDT liquids composition obtained at  $t_{\text{reaction}} = 0$  h, it can be observed that the  
446 concentration of aromatic C-H and C-C increases with temperature. In contrast, the occurrence of  
447 functional groups containing oxygen and aliphatic C follows the opposite trend (Figure 5). At  $t_{\text{reaction}} =$   
448 0 h, the aromatic carbon concentration was observed to increase with the reaction temperature,  
449 suggesting that thermal condensation occurs during reactor heating. Indeed, the UV absorption at  
450  $\lambda=290$  nm (Figure 6-B), characteristic of polyaromatic compounds, which can be formed by unstable  
451 products in the crude oil during heating, clearly increases as a function of temperature for  $T = 0$  h. As  
452 the reaction time increases, the concentration of aliphatic C increases together with a reduction of  
453 aromatic C as a consequence of hydrogenation, as confirmed by the H/C ratio increase from  $\approx 1.5$  at 0  
454 h to  $>1.6$  after 3 h for reaction (Figure 4). Additionally, the  $\frac{C_{\text{Aliphatic}}}{C_{\text{Aromatic}}}$  ratio increases more with the  
455 reaction time for higher temperatures due to the faster kinetics of the HDT reactions promoted by the  
456 catalyst. While HDT significantly reduced the concentration of aromatic C-H bonds, the concentration  
457 of aromatic C-C only decreased slightly at 375 °C and 390°C and even increased at 350 °C (Figure 5).  
458 Additionally, the  $\frac{C-C_{\text{Aromatic}}}{C_{\text{Aromatic}}} \cdot 6$  (where 6 refers to the number of carbon atoms in one aromatic ring),  
459 which accounts for the average number of C-C<sub>Aromatic</sub> bonds per aromatic ring, increased from 1.5 at 0  
460 h to 2.0 after 3 h of reaction. It should be mentioned that aromatic C-C bounds can result from  
461 polyaromatic hydrocarbons, partially hydrogenated polycyclic-aromatics, like tetraline, and alkylated  
462 aromatics, such as toluene. Aromatic ring hydrogenation in polyaromatic compounds decreases for  
463 each ring already hydrogenated in the molecule<sup>43,47,48</sup>. Indeed, our previous work screening the

464 upgrading of various HTL oils has already demonstrated that lignite crude oils were particularly rich in  
 465 aromatic compounds, which results in a significant concentration of naphthenes and cyclic  
 466 monoaromatic compounds after HDT<sup>49</sup>.



467  
 468 Figure 5. <sup>13</sup>C functional group composition of the liquid product obtained from HDT of lignite crude oil  
 469 at different reaction temperatures (350 °C, 375 °C, and 390 °C) and reaction times ( $t_{\text{reaction}}$ ).



471  
 472 **Figure 6.** A) Liquid product molecular weight ( $Mw_{\text{HC}}$ ) distribution determined by refraction index (RI),  
 473 and B) UV absorbance ( $\lambda = 290 \text{ nm}$ ) as a function of the compounds Mw. A hydrocarbon mixture with  
 474 Mw comprised between 86 g/mol and 1000 g/mol was used as a standard to determine  $Mw_{\text{HC}}$ .

475

476 The molecular weight ( $M_{w_{HC}}$ ) distribution of the HDT liquid products is shown in Figure 6A. At low  
477 reaction time, the  $M_{w_{HC}}$  distribution presented a maximum centered at  $\approx 200$  g/mol and a maximum  
478 molecular weight of 1 000 g/mol. As the reaction time increased, the compounds centered at 200  
479 g/mol progressively decreased as a new group of compounds centered at  $\approx 120$  g/mol appeared.  
480 Similarly, the higher molecular weight compounds progressively disappeared, and at 390 °C after 3 h  
481 of reaction, no compounds above 800 g/mol were detected. Indeed, the degree of  $M_{w_{HC}}$  reduction  
482 observed in the liquid products after HDT highly depended on the reaction time and temperature,  
483 with the average  $M_{w_{HC}}$  (Table S10) ranging from 243 g/mol to 160 g/mol. The average molecular  
484 weight of the liquid products is reported in Table S10.

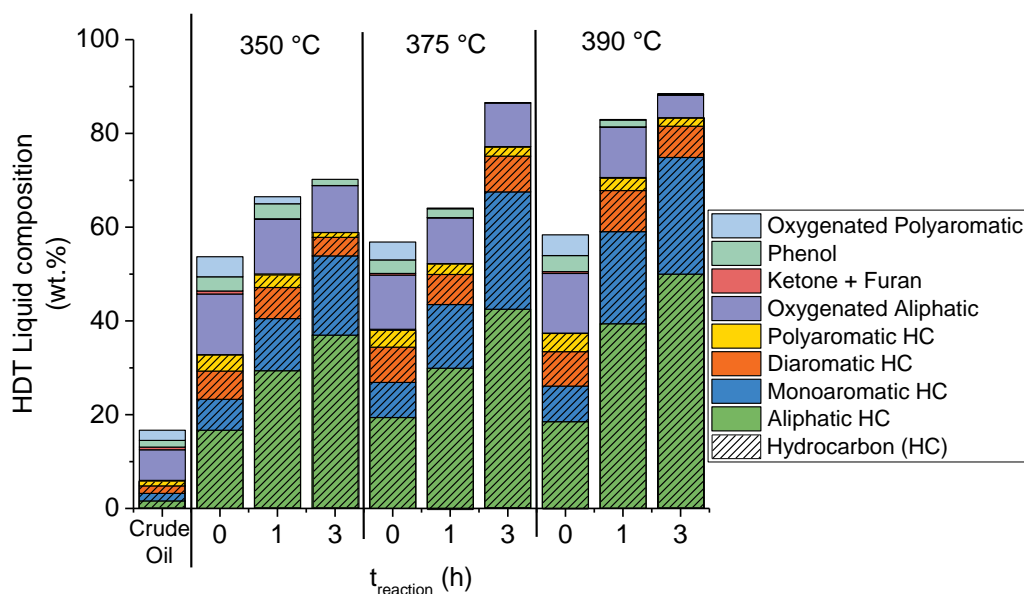
485 The removal of the heteroatom elements, i.e., O, N, and S, is considered to be the main responsible  
486 for the significant  $M_{w_{HC}}$  reduction since the cleavage of C-C bonds via hydrogenolysis is not  
487 predominant under the reaction conditions used in this study.

488 Figure 6B shows the absorbance at  $\lambda=290$  nm, characteristic of conjugated polyaromatic compounds,  
489 as a function  $M_{w_{HC}}$ . The absorbance decreases as a function of the reaction time due to the full or  
490 partial hydrogenation of the polyaromatic compounds. Still, Figure 6B clearly shows that  
491 polyaromatics undergo faster conversion in the first hour of a reaction than in the subsequent 2 h.  
492 Also, at all temperatures, the UV absorption for  $M_{w_{HC}} > 300$  g/mol decreases fast during HDT, with  
493 nearly all polyaromatics in this range being converted at  $T = 390$  °C after 3 h of reaction. However, the  
494 refraction index detector (RID – Figure 6A) clearly shows that the amount of compounds with a  $M_{w_{HC}}$   
495  $> 300$  g/mol are only reduced slightly during HDT. The difference between the two detectors suggests  
496 that higher  $M_{w_{HC}}$  polyaromatic compounds undergo hydrogenation faster. Indeed, Korre et al. studied  
497 the hydrogenation kinetic of multiple polyaromatic compounds identifying that the higher the number  
498 of conjugated rings, the faster the hydrogenation reaction rate<sup>50</sup>.



499 The composition of the liquid product, quantified by comprehensive GC×GC/FID (Figure 7), shows a  
500 progressive increase in the concentration of aliphatic and mono-aromatic hydrocarbon under harsher  
501 reaction conditions, as already suggested by <sup>13</sup>C NMR (Figure 5), SEC-DAD (Figure 6B), and elemental  
502 analysis (Figure 4) results. At the same time, the oxygenated compounds, such as phenols, ketones,  
503 furans, and other high molecular weight compounds, are progressively transformed. Furthermore, the  
504 concentration of compounds in the comprehensive GC×GC-FID analysis detection range, i.e., up to  
505 ≈C<sub>40</sub>, progressively increased with HDT reaction time and temperature, which is a consequence of the  
506 reduction of the Mw of the samples (Figure 6A). At 390 °C and 3 h of reaction, 88.4 wt.% of the HDT  
507 liquid product composition was quantified, with aliphatic and monoaromatic hydrocarbon, mainly  
508 composed of naphthenes and partially hydrogenated aromatics, respectively, contributing to ≈75%  
509 of the sample. Additionally, 9 wt.% of the liquid was composed of polyaromatic hydrocarbons with  
510 two or more aromatic rings. The high concentration of cyclic hydrocarbons in the liquid is a direct  
511 consequence of the aromatic nature of the products in the crude oil and, by extension, in lignite.  
512 Indeed, in our previous work, we demonstrated that the nature of the feedstock was crucial in  
513 determining the composition of the HDT liquid product and that lignite led to an HDT liquid rich in  
514 cyclic hydrocarbons<sup>49</sup>.

515 As mentioned before, lignite crude oil was already transformed during the 20 min heating stage of the  
516 reactor, as easily observable by the comprehensive GC×GC's significant compound detection boost,  
517 i.e., 16.7 wt.% to >56.7 wt.%. While the increase in aromatic content in the liquid showed that thermal  
518 phenomena caused at least part of the transformation, the rise in detectable aliphatic and  
519 monoaromatic hydrocarbon compounds suggests that catalytic HDT was also responsible for the  
520 transformation of the feedstock during the heating stage, indicating that lignite crude oil can undergo  
521 significant heteroatoms removal, even under relatively mild conditions.



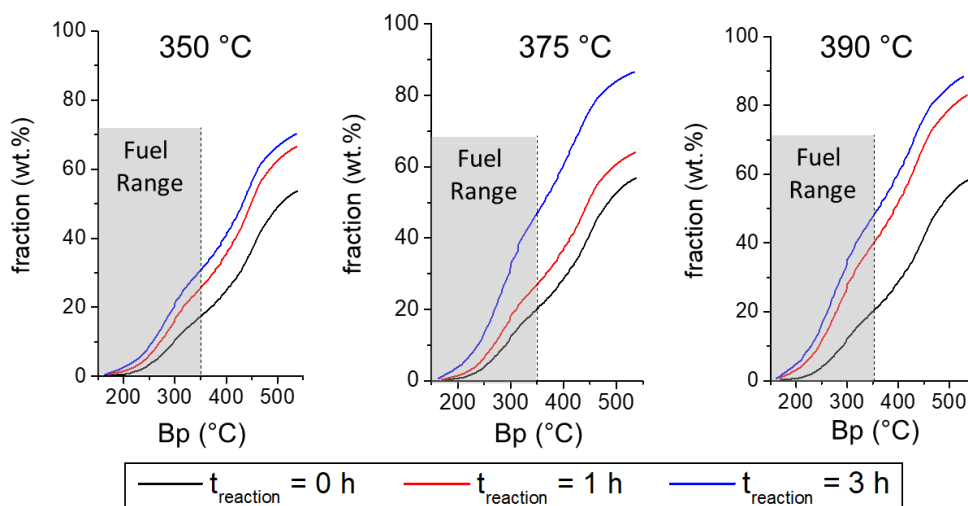
522

523 Figure 7. Composition of lignite crude oil and the HDT liquid as a function of the reaction temperature  
 524 (350 °C, 375 °C, and 390 °C) and reaction time ( $t_{\text{reaction}}$ ) detected by GCxGC-TOFMS (Figure S8) and  
 525 quantified by GCxGC-FID.

526

527 The distillation curves for the HDT liquid products are shown in Figure 8. As expected from the  
 528 reduction of Mw distribution observed in the SEC results (Figure 6A), the number of products in the  
 529 fuel range increases with the reaction temperature and time. While at 0h, the fuel range products  
 530 concentration is quite similar at all temperatures (17-20 wt.%), fuel yield quickly rises with the reaction  
 531 time (Table S11). It is worth mentioning that oxygenated products, like phenols, are present in the fuel  
 532 range products (boiling point < 350 °C) in all cases, except for the experiments performed at 375°C  
 533 and 390 °C after 3 h of reaction, which are exclusively composed of hydrocarbon molecules.  
 534 Additionally, diaromatic hydrocarbons are present in all cases and makeup  $\approx$  5 wt.% of the fuel range  
 535 products obtained at 375°C and 390 °C after 3 h of reaction. Additionally, the maximum fuel yield  
 536 obtained at 375°C and 390°C was 47.0 wt.% and 47.6 wt.%, respectively, showing that increasing the  
 537 HDT temperature has little effect on the overall fuel yield after the elimination of most heteroatoms  
 538 (Figure 4). Still, a slight variation in the composition of the fuel range products was observed (Tables

539 S12 and S13), with the test at 375°C yielding more products, i.e., 33.5 wt.% Vs 30.8 wt.%, in the middle  
 540 distillates range (Bp between 250°C and 350°C) and the test at 390°C being more selective for  
 541 kerosene (Bp between 175°C and 250 °C), i.e., 14.7 wt.% Vs. 11.9 wt.%. The increase in lower Bp  
 542 products observed at 390 °C might be associated with C-C hydrogenolysis, favored by a higher  
 543 temperature.



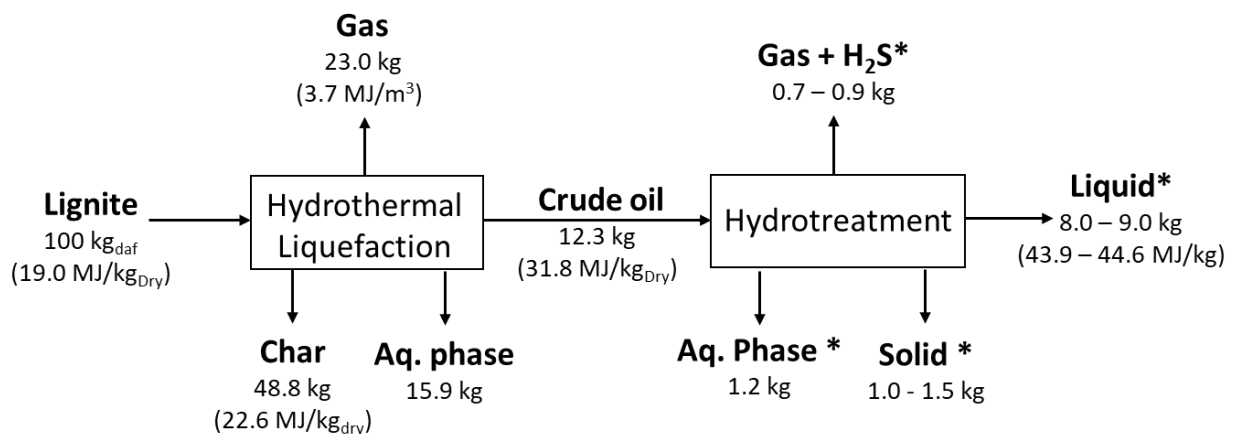
544  
 545 Figure 8. Distillation curve of the hydrotreatment liquid product as a function of reaction time ( $t_{\text{reaction}}$ ).  
 546 Fuel range: Bp < 350°C.

547  
 548 The overall mass balance of the process, shown in Figure 9, indicates that the HDT liquid yield obtained  
 549 from lignite under the HTL and HDT conditions used in this study is 8-9 wt.% and 47 wt.% of HDT liquid  
 550 products have a boiling point in the range of standard fuels, i.e., Bp < 350°C (Figure 8). The low yield  
 551 of crude oil during HTL, i.e., 12.3%, is responsible for the low overall conversion of lignite into fuel.  
 552 Indeed, the HDT liquid yield obtained in this study, i.e., 65-73 wt.%, was comparable to that in the  
 553 literature when upgrading HTL biocrudes produced from different feedstocks<sup>51-55</sup>. The low crude oil  
 554 yield can be explained by the experimental conditions used in the HTL process, as Liu et al. were able  
 555 to increase the crude oil production to 34 wt.% by using a lower HTL reaction time (5 min) and higher  
 556 temperature (440 °C). Additionally, the use of catalysts<sup>56</sup> and recycling the aqueous phase<sup>57</sup> are known

557 to increase crude yield during HTL. Therefore, adequate process optimization can orient a more  
 558 significant fraction of lignite towards fuel generation.

559 While lignite is not a green feedstock, its easily upgradable products obtained during HTL can be  
 560 beneficial under mixed hydrothermal liquefaction with greener feedstocks, like lignocellulosic  
 561 biomass, sewage sludge or algae, which yield crude oils more difficult to upgrade as proposed, for  
 562 instance, by Wang et al.<sup>58</sup>. Indeed, it was shown that the hydrothermal liquefaction of a mixture of  
 563 Jingou lignite, wheat straw, and plastic waste could provide a synergetic effect on oil yields. Synergetic  
 564 effects were also observed in the co-liquefaction of coal and polymers (polypropylene and  
 565 polystyrene) by Y. Shen et al.<sup>59</sup>. Finally, it is worth mentioning that the char from lignite HTL can be  
 566 further used for electricity production, the original purpose of lignite.

567



568

569 Figure 9. Block flow diagram of the transformation of lignite through hydrothermal liquefaction (HTL)  
 570 and subsequent hydrotreatment of the HTL crude oil. Mass basis = 100 kg of dry ash-free lignite (kg<sub>daf</sub>).  
 571 The values in brackets refer to the calorific value of the respective streams and were determined by  
 572 using the expression from<sup>60</sup>. \*values determined using the data from HDT performed during 3 h at  
 573 temperatures of 375°C and 390°C (Figures 3-A and 4).

574

575

576

#### 577 4. CONCLUSION

578 In several European countries, gross electricity is partly generated by the combustion of lignite. Here,  
579 we propose diverting one fraction of the lignite to produce kerosene and diesel through an HTL and  
580 single-stage HDT sequence. After HTL, only 12.3% of lignite was converted into crude oil. The low yield  
581 was attributed to the low temperature ( $T = 360\text{ °C}$ ) and high contact time ( $t_{\text{contact}} = 30\text{ min}$ ) used. The  
582 crude oil obtained from HTL was mainly composed of high molecular weight compounds, up to 2,000  
583 g/mol, which were particularly rich in oxygen (10.8 wt.%) and sulfur (2.4 wt.%). In addition to the crude  
584 oil, the lignite HTL also produced a char stream (48.8 wt.%) with the potential to be valorized for  
585 electricity production, the original purpose of lignite.

586 The hydrotreating experiments showed lignite's crude oil to be quite easily hydrotreated. Near  
587 complete S and O removal was achieved with a single HDT stage and using a milder pseudo-WHSV  
588 (equation 5) than those reported in the literature for pilot-scale bio-based crude oil HDT<sup>53,61</sup>. After  
589 HDT, despite a significant improvement in fuel quality, i.e., heteroatom removal and hydrogenation,  
590 substantial amounts of aromatic compounds, particularly monoaromatic and diaromatic compounds  
591 ( $\approx 45\%$  of fuel range products), are still present in all products. This suggests that further upgrading or  
592 harsher conditions, i.e., higher contact time and  $\text{H}_2$  pressure, are required. Indeed, aromatics have low  
593 cetane numbers, which can be detrimental for using the middle distillate in diesel fuels<sup>62</sup>. In addition  
594 to decreasing the aromatic content in the liquid product, our results showed that harshening HDT  
595 conditions did not significantly increase the fuel range products, suggesting that subsequent  
596 hydrocracking or using an HDT catalyst with acid properties might be necessary. Nevertheless, the  
597 crude oil obtained from the hydrothermal liquefaction of lignite has an excellent potential for  
598 producing hydrocarbon fuels, particularly when compared with other feedstocks typically used in the  
599 HTL process, like sewage sludge and algae<sup>46,63</sup>. Finally, it is important to mention that the presence of  
600 this aromatic fraction can be a benefit, acting as a polar solvent in the case of co-processing between  
601 HTL of lignite and less proper biogenic feedstocks, such as biomass or sewage sludge.

602 **5. Supporting information**

603 HTL experimental and product separation diagram; Catalyst composition; <sup>13</sup>C chemical shift  
604 attribution; GC×GC equipment configuration; HTL char composition; HTL gas yield; Crude oil <sup>13</sup>C NMR  
605 spectrum; crude oil GC/FPD<sup>+</sup> chromatogram; SEC/DAD of aromatic standards; spent catalyst carbon  
606 content; HDT deoxygenation, denitrogenation, and desulfurization results; HDT total fuel, kerosene,  
607 and middle distillates yield; GC×GC-TOFMS chromatographs.

608

609 **6. Acknowledgements**

610 The authors gratefully acknowledge the financial support of the European Commission Research  
611 Programme of the Research Fund for Coal and Steel for the project HyCon (Grant agreement: 899471).  
612 In the case of Polish authors, this scientific work is published as part of an international project co-  
613 financed by the program of the Ministry of Science and Higher Education entitled "PMW" in the years  
614 2020 -2023 agreement No. 5157/FBWiS/2020/2021/2

615

616

617

618 **7. References**

619

- 620 (1) Tollefson, J. What the War in Ukraine Means for Energy, Climate and Food. *Nature* **2022**, No.  
621 604, 232–233.
- 622 (2) IEA. *Renewables 2021: Analysis and Forecast to 2026*; Paris, 2021.  
623 <https://www.iea.org/reports/renewables-2021>.
- 624 (3) *Renewables 2019*; IEA: Paris, 2019. <https://www.iea.org/reports/renewables-2019>.
- 625 (4) Lignite Energy Council. *Uses and Benefits of Lignite*. [https://lignite.com/what-is-lignite/uses-](https://lignite.com/what-is-lignite/uses-and-benefits-of-lignite/)  
626 [and-benefits-of-lignite/](https://lignite.com/what-is-lignite/uses-and-benefits-of-lignite/).
- 627 (5) Eurostat. *Coal production and consumption up in 2022*.  
628 <https://ec.europa.eu/eurostat/web/products-eurostat-news/w/ddn-20230622-2>.
- 629 (6) Kershaw, J. R. Extraction of Victorian Brown Coals with Supercritical Water. *Fuel Processing*  
630 *Technology* **1986**, 13 (2), 111–124. [https://doi.org/10.1016/0378-3820\(86\)90053-6](https://doi.org/10.1016/0378-3820(86)90053-6).
- 631 (7) Deshpande, G. V.; Holder, G. D.; Bishop, A. A.; Gopal, J.; Wender, I. Extraction of Coal Using  
632 Supercritical Water. *Fuel* **1984**, 63 (7), 956–960. [https://doi.org/10.1016/0016-2361\(84\)90318-](https://doi.org/10.1016/0016-2361(84)90318-1)  
633 1.
- 634 (8) Hu, H.; Guo, S.; Hedden, K. Extraction of Lignite with Water in Sub- and Supercritical States.  
635 *Fuel Processing Technology* **1998**, 53 (3), 269–277. [https://doi.org/10.1016/S0378-](https://doi.org/10.1016/S0378-3820(97)00057-X)  
636 [3820\(97\)00057-X](https://doi.org/10.1016/S0378-3820(97)00057-X).
- 637 (9) Nikolopoulos, N.; Violidakis, I.; Karampinis, E.; Agraniotis, M.; Bergins, C.; Grammelis, P.;  
638 Kakaras, E. Report on Comparison among Current Industrial Scale Lignite Drying Technologies  
639 (A Critical Review of Current Technologies). *Fuel* **2015**, 155, 86–114.  
640 <https://doi.org/10.1016/j.fuel.2015.03.065>.
- 641 (10) Hartman, B. E.; Hatcher, P. G. Valuable Crude Oil from Hydrothermal Liquefaction of an  
642 Aliphatic Coal. *Energy Fuels* **2014**, 28 (12), 7538–7551. <https://doi.org/10.1021/ef5018708>.

- 643 (11) Liu, P.; Wang, L.; Zhou, Y.; Pan, T.; Lu, X.; Zhang, D. Effect of Hydrothermal Treatment on the  
644 Structure and Pyrolysis Product Distribution of Xiaolongtan Lignite. *Fuel* **2016**, *164*, 110–118.  
645 <https://doi.org/10.1016/j.fuel.2015.09.092>.
- 646 (12) Li, H.; Wu, S.; Wu, Y.; Wang, H.; Zhang, Z.; Huang, S.; Gao, J. Effects of Hydrothermal Treatment  
647 on Physico-Chemical Structures and Liquefaction Behaviors of Lignite. *Fuel* **2020**, *263*, 116636.  
648 <https://doi.org/10.1016/j.fuel.2019.116636>.
- 649 (13) Lelevic, A.; Souchon, V.; Geantet, C.; Lorentz, C.; Moreaud, M. Advanced Data Preprocessing  
650 for Comprehensive Two-Dimensional Gas Chromatography with Vacuum Ultraviolet  
651 Spectroscopy Detection. *Journal of Separation Science* **2021**, *44* (22), 4141–4150.  
652 <https://doi.org/10.1002/jssc.202100528>.
- 653 (14) Scanlon, J. T.; Willis, D. E. Calculation of Flame Ionization Detector Relative Response Factors  
654 Using the Effective Carbon Number Concept. *Journal of Chromatographic Science* **1985**, *23* (8),  
655 333–340. <https://doi.org/10.1093/chromsci/23.8.333>.
- 656 (15) Liu, C.; Li, J.; Lin, Y. Optimization Study of Sub/Supercritical Water Liquefaction of Lignite: Fast  
657 Liquefaction for High Bio-Oil Yield. *International Journal of Hydrogen Energy* **2019**, *44* (39),  
658 21406–21412. <https://doi.org/10.1016/j.ijhydene.2019.06.140>.
- 659 (16) Audu, M.; Wang, H.; Arellano, D.; Cheng, F.; Dehghanizadeh, M.; Jarvis, J. M.; Yan, J.; Brewer, C.  
660 E.; Jena, U. Ash-Pretreatment and Hydrothermal Liquefaction of Filamentous Algae Grown on  
661 Dairy Wastewater. *Algal Research* **2021**, *57*, 102282.  
662 <https://doi.org/10.1016/j.algal.2021.102282>.
- 663 (17) Chen, W.-T.; Qian, W.; Zhang, Y.; Mazur, Z.; Kuo, C.-T.; Scheppe, K.; Schideman, L. C.; Sharma,  
664 B. K. Effect of Ash on Hydrothermal Liquefaction of High-Ash Content Algal Biomass. *Algal*  
665 *Research* **2017**, *25*, 297–306. <https://doi.org/10.1016/j.algal.2017.05.010>.
- 666 (18) Liu, H.; Chen, Y.; Yang, H.; Gentili, F. G.; Söderlind, U.; Wang, X.; Zhang, W.; Chen, H. Conversion  
667 of High-Ash Microalgae through Hydrothermal Liquefaction. *Sustainable Energy Fuels* **2020**, *4*  
668 (6), 2782–2791. <https://doi.org/10.1039/C9SE01114E>.
- 669 (19) Liu, R.; Tian, W.; Kong, S.; Meng, Y.; Wang, H.; Zhang, J. Effects of Inorganic and Organic Acid  
670 Pretreatments on the Hydrothermal Liquefaction of Municipal Secondary Sludge. *Energy*  
671 *Conversion and Management* **2018**, *174*, 661–667.  
672 <https://doi.org/10.1016/j.enconman.2018.08.058>.
- 673 (20) Shafizadeh, A.; Shahbeig, H.; Nadian, M. H.; Mobli, H.; Dowlati, M.; Gupta, V. K.; Peng, W.; Lam,  
674 S. S.; Tabatabaei, M.; Aghbashlo, M. Machine Learning Predicts and Optimizes Hydrothermal  
675 Liquefaction of Biomass. *Chemical Engineering Journal* **2022**, *445*, 136579.  
676 <https://doi.org/10.1016/j.cej.2022.136579>.
- 677 (21) Oner, M.; Oner, G.; Bolat, E.; Yalin, G.; Kavlak, C.; Dincer, S. The Effect of Ash and Ash  
678 Constituents on the Liquefaction Yield of Turkish Lignites and Asphaltites. *Fuel* **1994**, *73* (10),  
679 1658–1666. [https://doi.org/10.1016/0016-2361\(94\)90147-3](https://doi.org/10.1016/0016-2361(94)90147-3).
- 680 (22) Vassilev, S. V.; Baxter, D.; Andersen, L. K.; Vassileva, C. G. An Overview of the Composition and  
681 Application of Biomass Ash. Part 1. Phase–Mineral and Chemical Composition and  
682 Classification. *Fuel* **2013**, *105*, 40–76. <https://doi.org/10.1016/j.fuel.2012.09.041>.
- 683 (23) Fedorova, N. I.; Ismagilov, Z. R. Ash Composition of Lignite. *Coke and Chemistry* **2019**, *62* (11),  
684 493–497. <https://doi.org/10.3103/S1068364X19110036>.
- 685 (24) Prado, G. H. C.; Rao, Y.; de Klerk, A. Nitrogen Removal from Oil: A Review. *Energy Fuels* **2017**,  
686 *31* (1), 14–36. <https://doi.org/10.1021/acs.energyfuels.6b02779>.
- 687 (25) Prado, G. H. C.; Rao, Y.; de Klerk, A. Nitrogen Removal from Oil: A Review. *Energy Fuels* **2017**,  
688 *31* (1), 14–36. <https://doi.org/10.1021/acs.energyfuels.6b02779>.
- 689 (26) ASTM D7566-22 -Standard Specification for Aviation Turbine Fuel Containing Synthesized  
690 Hydrocarbons. In *ASTM Volume 05.04: Petroleum Products, Liquid Fuels, And Lubricants (IV):*  
691 *D7412 – D8128*; ASTM, 2023; Vol. 05.04, p 2074.

- 692 (27) Stefanova, M.; Marinov, S. P.; Magnier, C. Aliphatic Biomarkers from Miocene Lignites  
693 Desulphurization. *Fuel* **1999**, *78* (12), 1395–1406. <https://doi.org/10.1016/S0016->  
694 2361(99)00068-X.
- 695 (28) Liu, J.; Wei, X.-Y.; Zhang, D.-D.; Li, Z.-K.; Lv, J.-H.; Wang, T.-M.; Gui, J.; Qu, M.; Guo, L.-L.; Zong,  
696 Z.-M.; Li, W.; Kong, L.-X. Characterization of Heteroatom-Containing Species in the Soluble  
697 Portion from the Ethanolysis of the Extraction Residue from Xinghe Lignite by Electrospray  
698 Ionization Fourier Transform Ion Cyclotron Resonance Mass Spectrometry. *Fuel* **2016**, *173*,  
699 222–229. <https://doi.org/10.1016/j.fuel.2016.01.059>.
- 700 (29) Liu, P.; Zhang, D. Effect of Hydrothermal Treatment on the Carbon Structure of Inner Mongolia  
701 Lignite. *International Journal of Coal Science & Technology* **2020**, *7* (3), 493–503.  
702 <https://doi.org/10.1007/s40789-020-00356-7>.
- 703 (30) Shi, Z.; Jin, L.; Zhou, Y.; Li, Y.; Hu, H. Effect of Hydrothermal Treatment on Structure and  
704 Liquefaction Behavior of Baiyinhua Coal. *Fuel Processing Technology* **2017**, *167*, 648–654.  
705 <https://doi.org/10.1016/j.fuproc.2017.08.015>.
- 706 (31) Maes, I. I.; Gryglewicz, G.; Machnikowska, H.; Yperman, J.; Franco, D. V.; Mullens, J.; Van  
707 Poucke, L. C. Rank Dependence of Organic Sulfur Functionalities in Coal. *Fuel* **1997**, *76* (5), 391–  
708 396. [https://doi.org/10.1016/S0016-2361\(97\)85515-9](https://doi.org/10.1016/S0016-2361(97)85515-9).
- 709 (32) Patwardhan, P. R.; Timko, M. T.; Class, C. A.; Bonomi, R. E.; Kida, Y.; Hernandez, H. H.; Tester, J.  
710 W.; Green, W. H. Supercritical Water Desulfurization of Organic Sulfides Is Consistent with  
711 Free-Radical Kinetics. *Energy Fuels* **2013**, *27* (10), 6108–6117.  
712 <https://doi.org/10.1021/ef401150w>.
- 713 (33) Meng, N.; Jiang, D.; Liu, Y.; Gao, Z.; Cao, Y.; Zhang, J.; Gu, J.; Han, Y. Sulfur Transformation in  
714 Coal during Supercritical Water Gasification. *Fuel* **2016**, *186*, 394–404.  
715 <https://doi.org/10.1016/j.fuel.2016.08.097>.
- 716 (34) Liao, J.; Fei, Y.; Marshall, M.; Chaffee, A. L.; Chang, L. Hydrothermal Dewatering of a Chinese  
717 Lignite and Properties of the Solid Products. *Fuel* **2016**, *180*, 473–480.  
718 <https://doi.org/10.1016/j.fuel.2016.04.027>.
- 719 (35) Liu, shucheng; Zhao, H.; Fan, T.; Zhou, J.; Liu, X.; Li, Y.; Zhao, G.; Wang, Y.; Zeng, M.  
720 Investigation on Chemical Structure and Hydrocarbon Generation Potential of Lignite in the  
721 Different Pretreatment Process. *Fuel* **2021**, *291*, 120205.  
722 <https://doi.org/10.1016/j.fuel.2021.120205>.
- 723 (36) Calkins, W. H. The Chemical Forms of Sulfur in Coal: A Review. *Fuel* **1994**, *73* (4), 475–484.  
724 [https://doi.org/10.1016/0016-2361\(94\)90028-0](https://doi.org/10.1016/0016-2361(94)90028-0).
- 725 (37) Fraga, G.; Batalha, N.; Kumar, A.; Bhaskar, T.; Konarova, M.; Perkins, G. Chapter 5 - Advances in  
726 Liquefaction for the Production of Hydrocarbon Biofuels. In *Hydrocarbon Biorefinery*; Maity, S.  
727 K., Gayen, K., Bhowmick, T. K., Eds.; Elsevier, 2022; pp 127–176. [https://doi.org/10.1016/B978-](https://doi.org/10.1016/B978-0-12-823306-1.00009-1)  
728 0-12-823306-1.00009-1.
- 729 (38) Yan, S.; Xia, D.; Liu, X. Beneficial Migration of Sulfur Element during Scrap Tire  
730 Depolymerization with Supercritical Water: A Molecular Dynamics and DFT Study. *Science of*  
731 *The Total Environment* **2021**, *776*, 145835. <https://doi.org/10.1016/j.scitotenv.2021.145835>.
- 732 (39) Saturnino, D. Compréhension de la relation entre la structure physico-chimique et l'activité  
733 des catalyseurs d'HDS vieillis, Université de Lyon, 2014.
- 734 (40) Zhu, C.; Gutiérrez, O. Y.; Santosa, D. M.; Kutnyakov, I.; Weindl, R.; Shi, H.; Wang, H. Impact of  
735 Coprocessing Biocrude with Petroleum Stream on Hydrotreating Catalyst Stability. *Energy Fuels*  
736 **2022**, *36* (16), 9133–9146. <https://doi.org/10.1021/acs.energyfuels.2c01748>.
- 737 (41) Benitez, A.; Ramirez, J.; Cruz-Reyes, J.; López Agudo, A. Effect of Alumina Fluoridation on  
738 Hydroconversion Ofn-Heptane on Sulfided NiW/Al<sub>2</sub>O<sub>3</sub>Catalysts. *Journal of Catalysis* **1997**, *172*  
739 (1), 137–145. <https://doi.org/10.1006/jcat.1997.1848>.
- 740 (42) WEISSER, O.; LANDA, S. 6 - HYDROGENATION, SYNTHESIS AND SOME REACTIONS OF  
741 INDIVIDUAL ORGANIC COMPOUNDS IN THE PRESENCE OF SULPHIDE CATALYSTS. In *Sulphide*



- 742 *Catalysts, their Properties and Applications*; WEISSER, O., LANDA, S., Eds.; Pergamon, 1973; pp  
743 118–284. <https://doi.org/10.1016/B978-0-08-017556-0.50011-3>.
- 744 (43) Girgis, M. J.; Gates, B. C. Reactivities, Reaction Networks, and Kinetics in High-Pressure  
745 Catalytic Hydroprocessing. *Ind. Eng. Chem. Res.* **1991**, *30* (9), 2021–2058.  
746 <https://doi.org/10.1021/ie00057a001>.
- 747 (44) Bello, S. S.; Wang, C.; Zhang, M.; Gao, H.; Han, Z.; Shi, L.; Su, F.; Xu, G. A Review on the Reaction  
748 Mechanism of Hydrodesulfurization and Hydrodenitrogenation in Heavy Oil Upgrading. *Energy*  
749 *Fuels* **2021**, *35* (14), 10998–11016. <https://doi.org/10.1021/acs.energyfuels.1c01015>.
- 750 (45) Xu, D.; Lin, G.; Guo, S.; Wang, S.; Guo, Y.; Jing, Z. Catalytic Hydrothermal Liquefaction of Algae  
751 and Upgrading of Biocrude: A Critical Review. *Renewable and Sustainable Energy Reviews*  
752 **2018**, *97*, 103–118. <https://doi.org/10.1016/j.rser.2018.08.042>.
- 753 (46) Cronin, D. J.; Subramaniam, S.; Brady, C.; Cooper, A.; Yang, Z.; Heyne, J.; Drennan, C.;  
754 Ramasamy, K. K.; Thorson, M. R. Sustainable Aviation Fuel from Hydrothermal Liquefaction of  
755 Wet Wastes. *Energies* **2022**, *15* (4), 1306. <https://doi.org/10.3390/en15041306>.
- 756 (47) Cooper, B. H.; Donnis, B. B. L. Aromatic Saturation of Distillates: An Overview. *Applied Catalysis*  
757 *A: General* **1996**, *137* (2), 203–223. [https://doi.org/10.1016/0926-860X\(95\)00258-8](https://doi.org/10.1016/0926-860X(95)00258-8).
- 758 (48) Stanislaus, A.; Cooper, B. H. Aromatic Hydrogenation Catalysis: A Review. *Catalysis Reviews*  
759 **1994**, *36* (1), 75–123. <https://doi.org/10.1080/01614949408013921>.
- 760 (49) Batalha, N.; Checa, R.; Lorentz, C.; Afanasiev, P.; Stańczyk, K.; Kapusta, K.; Laurenti, D.; Geantet,  
761 C. Lignite and Biomass Waste Hydrothermal Liquefaction Crude Upgrading by Hydrotreatment.  
762 *Energy Fuels* **2023**, *37* (14), 10506–10520. <https://doi.org/10.1021/acs.energyfuels.3c01550>.
- 763 (50) Korre, S. C.; Klein, M. T.; Quann, R. J. Polynuclear Aromatic Hydrocarbons Hydrogenation. 1.  
764 Experimental Reaction Pathways and Kinetics. *Ind. Eng. Chem. Res.* **1995**, *34* (1), 101–117.  
765 <https://doi.org/10.1021/ie00040a008>.
- 766 (51) Castello, D.; Haider, M. S.; Rosendahl, L. A. Catalytic Upgrading of Hydrothermal Liquefaction  
767 Biocrudes: Different Challenges for Different Feedstocks. *Renewable Energy* **2019**, *141*, 420–  
768 430. <https://doi.org/10.1016/j.renene.2019.04.003>.
- 769 (52) Sharma, K.; Castello, D.; Haider, M. S.; Pedersen, T. H.; Rosendahl, L. A. Continuous Co-  
770 Processing of HTL Bio-Oil with Renewable Feed for Drop-in Biofuels Production for Sustainable  
771 Refinery Processes. *Fuel* **2021**, *306*, 121579. <https://doi.org/10.1016/j.fuel.2021.121579>.
- 772 (53) Subramaniam, S.; Santosa, D. M.; Brady, C.; Swita, M.; Ramasamy, K. K.; Thorson, M. R.  
773 Extended Catalyst Lifetime Testing for HTL Biocrude Hydrotreating to Produce Fuel Blendstocks  
774 from Wet Wastes. *ACS Sustainable Chem. Eng.* **2021**, *9* (38), 12825–12832.  
775 <https://doi.org/10.1021/acssuschemeng.1c02743>.
- 776 (54) da Costa Magalhães, B.; Checa, R.; Lorentz, C.; Afanasiev, P.; Laurenti, D.; Geantet, C. Catalytic  
777 Hydroconversion of HTL Micro-Algal Bio-Oil into Biofuel over NiWS/Al<sub>2</sub>O<sub>3</sub>. *Algal Research*  
778 **2023**, *71*, 103012. <https://doi.org/10.1016/j.algal.2023.103012>.
- 779 (55) Magalhães, B. C.; Checa, R.; Lorentz, C.; Prévot, M.; Afanasiev, P.; Laurenti, D.; Geantet, C.  
780 Catalytic Hydrotreatment of Algal HTL Bio-Oil over Phosphide, Nitride, and Sulfide Catalysts.  
781 *ChemCatChem* **2023**, *15* (9), e202300025. <https://doi.org/10.1002/cctc.202300025>.
- 782 (56) Nagappan, S.; Bhosale, R. R.; Nguyen, D. D.; Chi, N. T. L.; Ponnusamy, V. K.; Woong, C. S.;  
783 Kumar, G. Catalytic Hydrothermal Liquefaction of Biomass into Bio-Oils and Other Value-Added  
784 Products – A Review. *Fuel* **2021**, *285*, 119053. <https://doi.org/10.1016/j.fuel.2020.119053>.
- 785 (57) Watson, J.; Wang, T.; Si, B.; Chen, W.-T.; Aierzhati, A.; Zhang, Y. Valorization of Hydrothermal  
786 Liquefaction Aqueous Phase: Pathways towards Commercial Viability. *Progress in Energy and*  
787 *Combustion Science* **2020**, *77*, 100819. <https://doi.org/10.1016/j.pecs.2019.100819>.
- 788 (58) Wang, B.; Huang, Y.; Zhang, J. Hydrothermal Liquefaction of Lignite, Wheat Straw and Plastic  
789 Waste in Sub-Critical Water for Oil: Product Distribution. *Journal of Analytical and Applied*  
790 *Pyrolysis* **2014**, *110*, 382–389. <https://doi.org/10.1016/j.jaap.2014.10.004>.

- 791 (59) Shen, Y.; Wu, H.; Pan, Z. Co-Liquefaction of Coal and Polypropylene or Polystyrene in Hot  
792 Compressed Water at 360–430°C. *Fuel Processing Technology* **2012**, *104*, 281–286.  
793 <https://doi.org/10.1016/j.fuproc.2012.05.023>.
- 794 (60) Channiwala, S. A.; Parikh, P. P. A Unified Correlation for Estimating HHV of Solid, Liquid and  
795 Gaseous Fuels. *Fuel* **2002**, *81* (8), 1051–1063. [https://doi.org/10.1016/S0016-2361\(01\)00131-4](https://doi.org/10.1016/S0016-2361(01)00131-4).
- 796 (61) Verdier, S.; Mante, O. D.; Hansen, A. B.; Poulsen, K. G.; Christensen, J. H.; Ammtizboll, N.;  
797 Gabrielsen, J.; Dayton, D. C. Pilot-Scale Hydrotreating of Catalytic Fast Pyrolysis Biocrudes:  
798 Process Performance and Product Analysis. *Sustainable Energy Fuels* **2021**, *5* (18), 4668–4679.  
799 <https://doi.org/10.1039/D1SE00540E>.
- 800 (62) Song, C.; Ma, X. New Design Approaches to Ultra-Clean Diesel Fuels by Deep Desulfurization  
801 and Deep Dearomatization. *Applied Catalysis B: Environmental* **2003**, *41* (1), 207–238.  
802 [https://doi.org/10.1016/S0926-3373\(02\)00212-6](https://doi.org/10.1016/S0926-3373(02)00212-6).
- 803 (63) Hao, B.; Xu, D.; Jiang, G.; Sabri, T. A.; Jing, Z.; Guo, Y. Chemical Reactions in the Hydrothermal  
804 Liquefaction of Biomass and in the Catalytic Hydrogenation Upgrading of Biocrude. *Green*  
805 *Chem.* **2021**, *23* (4), 1562–1583. <https://doi.org/10.1039/D0GC02893B>.  
806